Proceedings of the 2001 IEEE/RSJ
International Conference on Intelligent Robots and Systems
Maui, Hawaii, USA, Oct. 29 - Nov. 03, 2001

The 3D Linear Inverted Pendulum Mode: A simple modeling for a biped walking pattern generation

Shuuji Kajita, Fumio Kanehiro, Kenji Kaneko, Kazuhito Yokoi and Hirohisa Hirukawa

National Institute of Advanced Industrial Science and Technology (AIST)
Umezono 1-1-1, Tsukuba Ibaraki 305, Japan
E-mail: s.kajita@aist.go.jp

Abstract

For 3D walking control of a biped robot we analyze the dynamics of a three-dimensional inverted pendulum in which motion is constrained to move along an arbitrarily defined plane. This analysis leads us a simple linear dynamics, the Three-Dimensional Linear Inverted Pendulum Mode (3D-LIPM). Geometric nature of trajectories under the 3D-LIPM and a method for walking pattern generation are discussed. A simulation result of a walking control using a 12 d.o.f. biped robot model is also shown.

1 Introduction

Research on humanoid robots and biped locomotion is currently one of the most exciting topics in the field of robotics and there exist many ongoing projects. Although some of those works have already demonstrated very reliable dynamic biped walking[5, 15], we believe it is still important to understand the theoretical background of biped locomotion.

A lot of researches dedicated to the biped walking pattern generation can be classified into two categories. The first group uses precise knowledge of dynamic parameter of a robot e.g. mass, location of center of mass and inertia of each link to prepare walking patterns. Therefore, it mainly relies on the accuracy of the model data [15, 5, 12, 6].

Contrary, the second group uses limited knowledge of dynamics e.g. location of total center of mass, total angular momentum, etc. Since the controller knows little about the system structure, this approach much relies on a feedback control [14, 1, 11, 17, 7, 2, 13].

In this paper we take a standpoint of the second approach, and introduce a new modeling which represents a robot dynamics with limited parameters. The modeling, the Three-Dimensional Linear Inverted Pendulum Mode (3D-LIPM) is derived from a general three-dimensional inverted pendulum whose motion is constrained to move along an arbitrarily defined plane. It allows a separate controller design for the sagittal (x-z) and the lateral (y-z) motion and simplifies a walking pattern generation a great deal.

2 Derivation of 3D Linear Inverted Pendulum Mode

2.1 Motion equation of a 3D inverted pendulum

When a biped robot is supporting its body on one leg, its dominant dynamics can be represented by a single inverted pendulum which connects the supporting foot and the center of mass of the whole robot. Figure 1 depicts such an inverted pendulum consisting of a point mass and a massless telescopic leg. The position of the point mass $\boldsymbol{p} = (x, y, z)$ is uniquely specified by a set of state variables $\boldsymbol{q} = (\theta_r, \theta_p, r)$.

$$x = rS_p, \quad (1)$$
$$y = -rS_r, \quad (2)$$
$$z = rD, \quad (3)$$

$$S_r \equiv \sin\theta_r, S_p \equiv \sin\theta_p, D \equiv \sqrt{1 - {S_r}^2 - {S_p}^2}.$$

Let (τ_r, τ_p, f) be the actuator torque and force associated with the state variables (θ_r, θ_p, r). With these inputs, the equation of motion of the 3D inverted pendulum in Cartesian coordinates is given as follows.

$$m \begin{pmatrix} \ddot{x} \\ \ddot{y} \\ \ddot{z} \end{pmatrix} = (\mathrm{J}^{\mathrm{T}})^{-1} \begin{pmatrix} \tau_r \\ \tau_p \\ f \end{pmatrix} + \begin{pmatrix} 0 \\ 0 \\ -mg \end{pmatrix}, \quad (4)$$

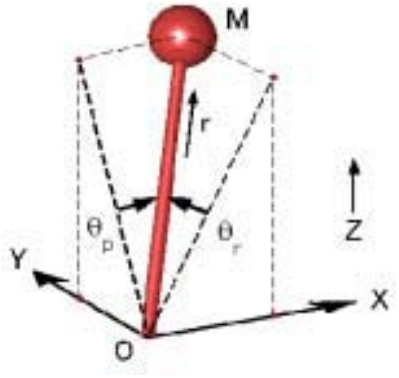

Figure 1: *3D Pendulum*

where m is the mass of the pendulum and g is gravity acceleration. The structure of the Jacobian J is

$$\mathrm{J} = \frac{\partial \boldsymbol{p}}{\partial \boldsymbol{q}} = \begin{pmatrix} 0 & rC_p & S_p \\ -rC_r & 0 & -S_r \\ -rC_rS_r/D & -rC_pS_p/D & D \end{pmatrix}, \tag{5}$$

$$C_r \equiv \cos\theta_r, C_p \equiv \cos\theta_p.$$

To erase the inversed Jacobian that appears in (4), let us multiply the matrix J^{T} from the left.

$$m \begin{pmatrix} 0 & -rC_r & -rC_rS_r/D \\ rC_p & 0 & -rC_pS_p/D \\ S_p & -S_r & D \end{pmatrix} \begin{pmatrix} \ddot{x} \\ \ddot{y} \\ \ddot{z} \end{pmatrix} = \begin{pmatrix} \tau_r \\ \tau_p \\ f \end{pmatrix} - mg \begin{pmatrix} -rC_rS_r \\ -rC_pS_p/D \\ D \end{pmatrix} \tag{6}$$

Using the first row of this equation and multiplying D/C_r we get

$$m(-rD\ddot{y} - rS_r\ddot{z}) = \frac{D}{C_r}\tau_r + rS_rmg. \tag{7}$$

By substituting kinematic relationship of equations (2) and (3), we get a good-looking equation that describes the dynamics along the y-axis.

$$m(-z\ddot{y} + y\ddot{z}) = \frac{D}{C_r}\tau_r - mgy \tag{8}$$

A similar procedure for the second row of (6) yields the equation for the dynamics along the x-axis.

$$m(z\ddot{x} - x\ddot{z}) = \frac{D}{C_p}\tau_p + mgx \tag{9}$$

2.2 3D Linear Inverted Pendulum Mode

Although the moving pattern of the pendulum has vast possibilities, we want to select a class of motion that would be suitable for walking. For this reason, we apply constraints to limit the motion of the pendulum. The first constraint limits the motion in a plane with given normal vector $(k_x, k_y, -1)$ and z intersection z_c.

$$z = k_x x + k_y y + z_c \tag{10}$$

For a robot walking on a rugged terrain, the normal vector should match the slope of the ground and the z intersection should be the expected average distance of the center of the robot's mass from the ground. For further calculation, we prepare the second derivatives of (10).

$$\ddot{z} = k_x\ddot{x} + k_y\ddot{y} \tag{11}$$

Substituting these constraints into equations (8) and (9), we obtain the dynamics of the pendulum under the constraints. From straightforward calculations we get

$$\ddot{y} = \frac{g}{z_c}y - \frac{k_1}{z_c}(x\ddot{y} - \ddot{x}y) - \frac{1}{mz_c}u_r, \tag{12}$$

$$\ddot{x} = \frac{g}{z_c}x + \frac{k_2}{z_c}(x\ddot{y} - \ddot{x}y) + \frac{1}{mz_c}u_p, \tag{13}$$

where u_r, u_p are new virtual inputs which are introduced to compensate input nonlinearity.

$$\tau_r = \frac{C_r}{D}u_r \tag{14}$$

$$\tau_p = \frac{C_p}{D}u_p \tag{15}$$

In the case of the walking on a flat plane, we can set the horizontal constraint plane $(k_x = 0, k_y = 0)$ and we obtain

$$\ddot{y} = \frac{g}{z_c}y - \frac{1}{mz_c}u_r, \tag{16}$$

$$\ddot{x} = \frac{g}{z_c}x + \frac{1}{mz_c}u_p. \tag{17}$$

In the case of the walking on a slope or stairs where $k_x, k_y \neq 0$, we need another constraint. From $x\times(12)+y\times(13)$ we see

$$x\ddot{y} - \ddot{x}y = \frac{-1}{mz}(u_rx + u_py). \tag{18}$$

Therefore, we have the same dynamics of (16) and (17) in the case of an inclined constraint plane by introducing the following new constraint about the inputs.

$$u_rx + u_py = 0 \tag{19}$$

Equations (16) and (17) are independent linear equations. The only parameter which governs those dynamics is z_c, i.e., the z intersection of the constraint plane and the inclination of the plane never affects the horizontal motion. Note that the original dynamics were nonlinear and we derived linear dynamics without using any approximation.

Let us call this the Three-Dimensional Linear Inverted Pendulum Mode (3D-LIPM). The first author and Tani introduced a two-dimensional version of this dynamics mode[7] in 1991, and Hara, Yokokawa and Sadao extended it to three dimensions in the case of zero input torque[4] in 1997.

3 Nature of the 3D Linear Inverted Pendulum Mode

In this section, we examine nature of trajectories under the 3D-LIPM with zero input torques ($u_r = u_p = 0$).

$$\ddot{y} = \frac{g}{z_c} y \tag{20}$$

$$\ddot{x} = \frac{g}{z_c} x \tag{21}$$

With a given initial condition, these equations determine a trajectory in 3D space. Figure 2 shows two examples.

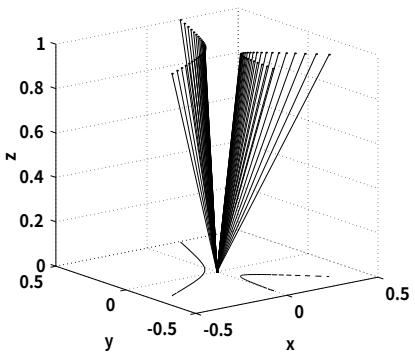

Figure 2: *3D Linear Inverted Pendulum Mode*

3.1 Similarity and difference with gravity field

We can regard that equations (20) and (21) represent a force field for a unit mass.

$$f = \frac{g}{z_c} r \tag{22}$$

A unit mass is driven by a force vector of magnitude f that is proportional to the distance r between the mass and the origin. The force magnitude can be distributed into x and y element as follows.

$$f_y = f(\frac{y}{r}) = \frac{g}{z_c} y \tag{23}$$

$$f_x = f(\frac{x}{r}) = \frac{g}{z_c} x \tag{24}$$

Equation (22) reminds us the celestial mechanics under the gravity field. In this case, the force magnitude is

$$f_G = -\frac{k_G}{r^2}, \tag{25}$$

where k_G is a parameter determined from the gravity constant and the mass of the gravity source. Both in the equations (22) and (25), the force vectors are parallel to the position vectors from the origin to the mass. This results well-known Kepler's second law of planetary motion: areal velocity conservation.

Let us see how the force of gravity can be separated into x and y direction.

$$f_{Gx} = \frac{x}{r}(-\frac{k_G}{r^2}) = -\frac{x k_G}{(x^2+y^2)^{3/2}} \tag{26}$$

$$f_{Gy} = \frac{y}{r}(-\frac{k_G}{r^2}) = -\frac{y k_G}{(x^2+y^2)^{3/2}} \tag{27}$$

Since x affects f_{Gy} and y affects f_{Gx}, we must always treat these two equations as a set. Contrarily, the x and y element of the 3D-LIPM can be treated independently at all times. This gives us great advantages in analyzing and in designing walking patterns as we will see in the following sections.

3.2 Geometry of the trajectory

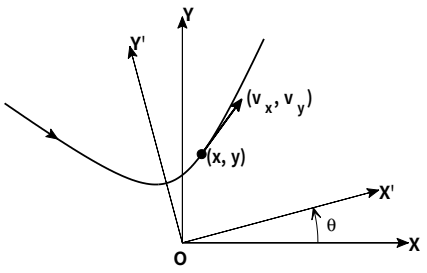

Figure 3: *3D-LIPM projected onto XY plane*

Figure 3 shows a 3D-LIPM trajectory which is projected onto XY plane. Motions along Y and X are governed by the equations (20) and (21) respectively. By integrating each equation, we obtain a time invariant parameter named the *orbital energy* [7].

$$E_y = -\frac{g}{2z_c}y^2 + \frac{1}{2}\dot{y}^2 \quad (28)$$

$$E_x = -\frac{g}{2z_c}x^2 + \frac{1}{2}\dot{x}^2 \quad (29)$$

In Figure 3, it is shown another coordinate frame $X'Y'$ which rotates θ from the original frame XY. Since the 3D-LIPM is a dynamics under the central force field as discussed in the last section, the new frame $X'Y'$ also gives a proper representation of the 3D-LIPM. The new orbital energy is calculated as,

$$E'_x = -\frac{g}{2z_c}(cx + sy)^2 + \frac{1}{2}(c\dot{x} + s\dot{y})^2, \quad (30)$$

$$E'_y = -\frac{g}{2z_c}(-sx + cy)^2 + \frac{1}{2}(-s\dot{x} + c\dot{y})^2, \quad (31)$$

where $c \equiv \cos\theta, s \equiv \sin\theta$. By simple calculations we can verify that the total energy of the system does not change by the way of the coordinate setting.

$$E'_x + E'_y = E_x + E_y = constant. \quad (32)$$

When the Y'-axis corresponds to the axis of symmetry like in Figure 3, E'_x and E'_y become maximum and minimum respectively. Therefore, we can calculate the axis of symmetry by solving the following equation.

$$\frac{\partial E'_x}{\partial \theta} = A(s^2 - c^2) + Bsc = 0, \quad (33)$$

where

$$A \equiv (g/z_c)xy - \dot{x}\dot{y}, \quad (34)$$

$$B \equiv (g/z_c)(x^2 - y^2) - (\dot{x}^2 - \dot{y}^2). \quad (35)$$

The solution is, when $B \neq 0$

$$\theta = \frac{1}{2}\tan^{-1}(2A/B), \quad (36)$$

when $B = 0, A \neq 0$

$$\theta = \pi/4, \quad (37)$$

when $B = 0, A = 0$

$$\theta = atan2(y, x). \quad (38)$$

If the Y-axis happen to be already the axis of symmetry, θ should be zero. From equations (36) and (34), following condition must be satisfied (Since $B = 0$ rarely happens, we do not consider eq.(37) and (38)).

$$(g/z_c)xy - \dot{x}\dot{y} = 0 \quad (39)$$

Using this equation, we can calculate the geometric shape of the 3D-LIPM. By substituting eq.(28) and (29),

$$(g/z_c)^2x^2y^2 = \dot{x}^2\dot{y}^2$$
$$= (2E_x + (g/z_c)x^2)(2E_y + (g/z_c)y^2).$$

The final form is a simple quadratic equation.

$$\frac{g}{2z_cE_x}x^2 + \frac{g}{2z_cE_y}y^2 + 1 = 0 \quad (40)$$

Since $E_x > 0$ and $E_y < 0$, eq.(40) forms a hyperbolic curve.

Hyperbolic curves also appear in Kepler motion, and one of its examples is a *swing by flight* of the Voyager 1 spacecraft approached Jupiter in 1979 [16]. It seems interesting that we obtained same shape of trajectory from a totally different potential field.

4 3D walking pattern generation

4.1 Outline

Figure 4 shows an example of a walking pattern based on the 3D-LIPM. In this paper we assume support leg exchange of constant pace. To change the walking speed and direction, the robot modifies foot placements (shown as small circles in Figure 4).

When we project the walking motion onto X and Y-axis, we observe decoupled motions governed by equations (21) and (20) (Figure 5). Each motion follows the 2D version of the Linear Inverted Pendulum Mode that we described in the former paper [7].

4.2 Pattern generation along a local axis

Now the problem becomes a control of the motion along X or Y-axis for each step. Let us assume that the robot is repeating single support phase of duration T_s and double support phase of duration T_{dbl}.

Figure 6 illustrates successive steps in X-direction. The initial body state $(x_i^{(n)}, v_i^{(n)})$ and the final body state $(x_f^{(n)}, v_f^{(n)})$ have the following relationship.

$$\begin{pmatrix} x_f^{(n)} \\ v_f^{(n)} \end{pmatrix} = \begin{pmatrix} C_T & T_cS_T \\ S_T/T_c & C_T \end{pmatrix} \begin{pmatrix} x_i^{(n)} \\ v_i^{(n)} \end{pmatrix} \quad (41)$$

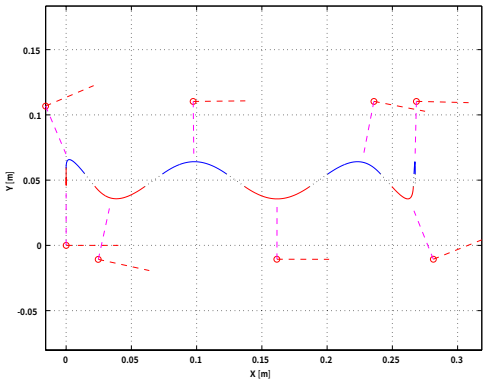

Figure 4: *Walking pattern generated from the 3D-LIPM. A robot takes seven steps from left to right. Motion of the tip of the inverted pendulum is shown as pieces of hyperbolic curves (solid lines). We assume that the robot is in double support and moves on a straight line between each support phase (dotted lines). Small circles are foot places and dashed lines indicate primary axes of hyperbolic curve.*

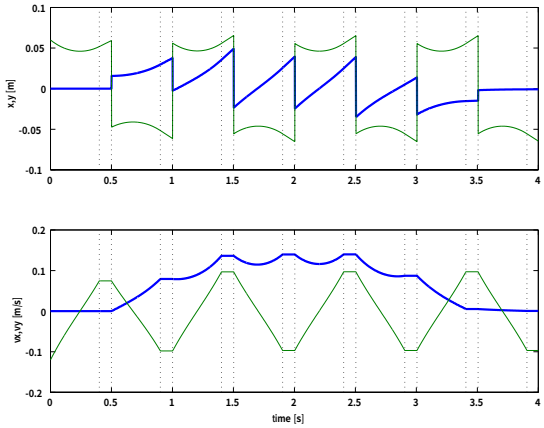

Figure 5: *XY-position and velocity in a walk of the figure 4. The tick line shows x motion and the thin line shows y motion. The position graphs jump the distance of the step length at each support foot exchange, since we are taking an origin at a foot place of each support. The vertical dotted lines indicate the time of the supporting mode change. In this walking pattern, the robot is taking 0.4s for single support and 0.1s for double support.*

$$C_T \equiv \cosh(T_s/T_c), S_T \equiv \sinh(T_s/T_c)$$

To control the walking speed, we must change the foothold (point E) to modify the initial condition of the support phase (D'→F). When the desired status at the end of support (point F) is given as (x_d, v_d) we can define error norm with certain weight $a, b > 0$ as

$$N \equiv a(x_d - x_f^{(2)})^2 + b(v_d - v_f^{(2)})^2.$$

By substituting eq.(41) into this equation and calculating the foothold of $x_i^{(2)}$ which minimizes N, we obtain a proper control law.

$$x_i^{(2)} = (aC_T(x_d - S_T T_c v_d) + bS_T/T_c(v_d - C_T v_f))/D_T \quad (42)$$

$$D_T \equiv aC_T^2 + b(S_T/T_c)^2$$

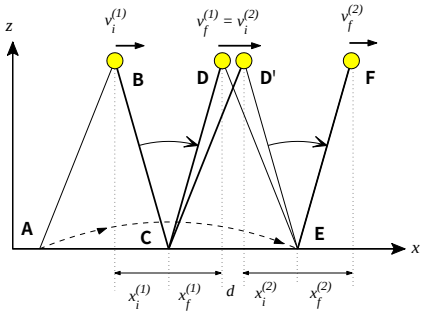

Figure 6: *Two successive steps in the sagittal plane are illustrated. The body travels from B to D in the single-leg support phase, then moves from D to D' in the double-leg support phase with constant speed $v_f^{(1)}$, and then travels D' to F in the second single-support phase. While the body moves from B to D, the tip of the swing leg travels from A to E (dashed curved line). By changing the position of E we can control the final body speed $v_f^{(2)}$ at the point F. Except for our inserted double-support phase, this is the same idea proposed by Miura and Shimoyama [10].*

To determine the foothold E, we also need the distance that body travels in the double support. The distance is

$$d = v_f^{(1)} T_{dbl}. \quad (43)$$

The motion of the swing leg is planned to arrive at the point E at the expected touchdown time (dashed curve from A to E in Figure 6).

4.3 Control of walking direction

To specify the walking direction, we rotates the reference XY-frame for step to step (See Figure 3). The control of eq.(42) automatically shapes the robot motion to follow the given frame of reference. Figure 7 illustrates a walking along a circle. In this walking pattern, the reference frame is rotated $\pi/10$ rad so that the robot returns the stating point with 20 steps.

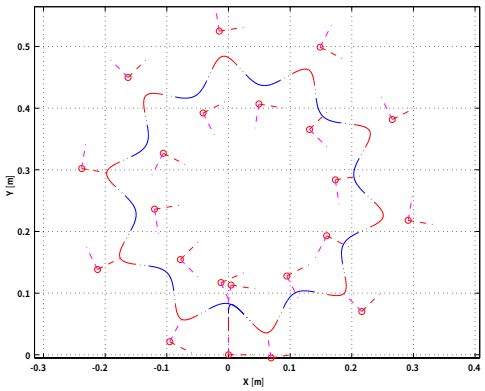

Figure 7: *Walk on a circle*

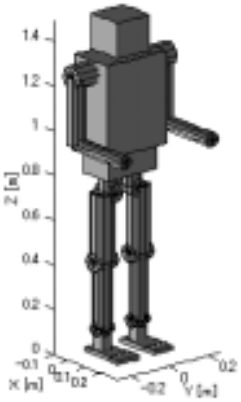

Figure 8: *A Humanoid Robot model. Total mass of the robot is 56kgs and the center of mass is located 0.542m in the height from the floor level. The robot has 6 d.o.f. for each leg but the arms and the head do not contain any joints (modeled as one block with the body).*

5 Simulation of humanoid walking

The 3D-LIPM has been already applied to a non-humanoid type biped robot that has telescopic legs. Though the robot could perform 3D dynamic biped walking without using prepared trajectory walking direction control was not yet considered [8].

In this paper, we examine a simulated humanoid robot whose motion is generated by the 3D-LIPM. Figure 8 shows the outlook of the robot used in the simulation. The robot has 6 d.o.f. for each leg but the arms and the head are modeled as one block with the body. Table 1 shows important physical parameters that was determined by considering an actual mechanical design. The size of the foot is 0.21m × 0.1m (length × width). Total mass of the robot is 56kgs and the center of mass is located 0.542m in the height from the floor level.

For the dynamic simulation we used the *OpenHRP simulator* which was developed in METI's humanoid robotics project [9]. The walking pattern of Figure 7 was used as a reference input to the robot and the center of mass of the robot body was controlled to follow this. To walk on a flat floor, the body height was kept

Table 1: *Important link parameters*

length [m]	
width of pelvis†	0.12
thigh link	0.3
schank link	0.3
ankle-sole distance	0.11
foot length	0.21
foot width	0.1
weight [kg]	
body	20
crotch yaw	1
crotch roll	2
thigh	5
shank	4
ankle pitch	3
foot	3
moment of inertia of the body [kgm^2]	
I_{xx}	0.5548
I_{yy}	0.4882
I_{zz}	0.1417

† distance between the right and left hip joints

constant. The reference joint angles and speeds were calculated by inverse kinematics so that the position and the velocity of the feet with respect to the body correspond to the specified motion. Finally, the reference joint angles and speeds were realized by a PD feedback controller.

Furthermore, we must consider the body and the foot rotation around z-axis. Although the walking pattern of Figure 7 is assuming an ideal robot that can step towards any direction at all time, the robot of Figure 8 has the limit of joint angles and it must avoid collision between the left and the right legs. For this reason we designed additional pattern for the foot orientation with respect to the body so that the body faces instantaneous walking direction in the middle of each support.

Figure 9 shows the snapshots of the simulation and Figure 10 shows the body trajectory and foot placements. We see that the trajectory of the humanoid robot did not close a circle at the 20th steps. This causes from a small foot slip occurred in each support (the friction coefficient between the foot and the floor: $\mu = 0.5$). In Figure 10, we can see the slip as blur of the footholds that should be fixed points. At the same time, the foot slips around z-axis and that diverted the robot from the planned walking direction.

Despite of the error caused by slip of the feet, it is important that a stable dynamic walk was realized by the 3D-LIPM trajectories. We believe the error can be reduced by introducing additional feedback control to the 3D-LIPM system. For example, Fujimoto and Kawamura proposed a feedback compensation of yaw axis rotation by arm swing motion [3]. By introducing such methods, we can expect more accurate walking direction control.

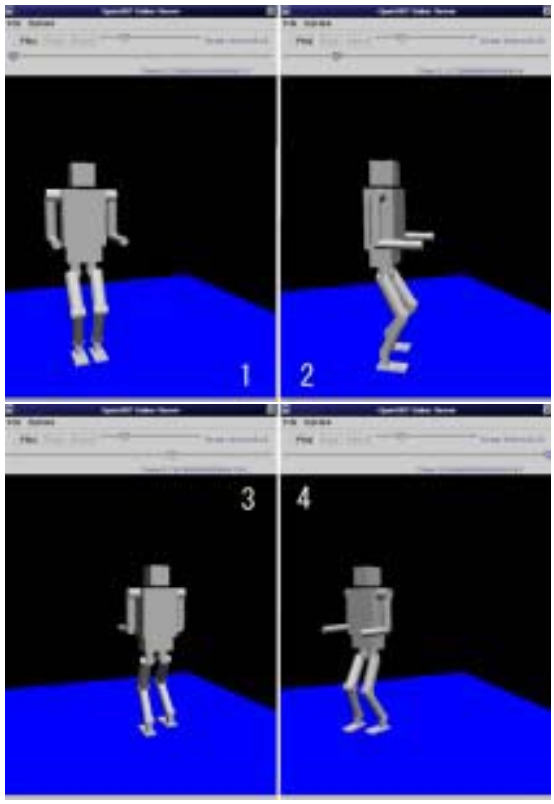

Figure 9: *Snapshots of humanoid simulator*

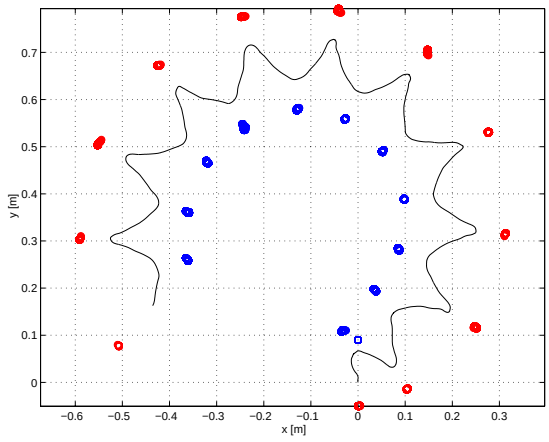

Figure 10: *Hip motion and foot place*

6 Summary and Conclusions

In this paper, we introduced the Three-Dimensional Linear Inverted Pendulum Mode (3D-LIPM) that is useful for walking control in a 3D space. We discussed a nature of the 3D-LIPM and proposed a simple walking pattern generation that can specify walking speed and direction. The walking pattern was tested on a 12 d.o.f. humanoid robot in a dynamic simulator, and a dynamically stable walk along a circle was successfully simulated.

Acknowledgments

This research was supported by the Humanoid Robotics Project of the Ministry of Economy, Trade

and Industry, through the Manufacturing Science and Technology Center.

References

[1] Furusho, J. and Sano, A., "Sensor-based control of a nine-link biped," Int. J. Robotics Research, vol,9, no.2, pp.83-98, Apr. 1990.

[2] Fujimoto, Y. and Kawamura, A., "Three Dimensional Digital Simulation and Autonomous Walking Control for Eight-Axis Biped Robot," Proc. of the 1995 ICRA, pp.2877-2884, 1995.

[3] Fujimoto, Y. and Kawamura, A., "Robust Control of Biped Walking Robot with Yaw Moment Compensation by Arm Motion," Proc. Asian Control Conference (ASCC'97), vol.3, pp.327-330,Seoul, 1997.

[4] Hara,K., Yokokawa,R. and Sadao, K., "Dynamic Control of Biped Locomotion Robot for Disturbance on Lateral Plane," Proc. of The Japan Society of Mechanical Engineers 72nd kansai meeting, pp.10-37–10-38, 1997 (in Japanese).

[5] Hirai, K., Hirose,M., Haikawa, Y. and Takenaka, T., "The Development of Honda Humanoid Robot," Proc. of the 1998 ICRA, pp.1321-1326, 1998.

[6] Huang, Q., Kajita, S. et.al, "A High Stability, Smooth Walking Pattern for a Biped Robot," Proc. of the 1999 ICRA, pp.65-71, 1999.

[7] Kajita,S. and Tani, K., "Study of Dynamic Biped Locomotion on Rugged Terrain," Proc. of the 1991 ICRA, pp.1405-1410, 1991.

[8] Kajita,S., Matsumoto,O. and Saigo, M., "Real-time 3D walking pattern generation for a biped robot with telescopic legs," Proc. of the 2001 ICRA, pp.2299-2308, 2001.

[9] Kanehiro,F., Miyata,N., Kajita,S., Fujiwara,K., Hirukawa,H., Nakamura,Y., Yamane,K. et.al, "Virtual Humanoid Robot Platform to Develop Controllers of Real Humanoid Robots without Porting," Proc. of the IROS 2001, (to apprear).

[10] Miura,H. and Shimoyama, I., "Dynamic walk of a biped," International Journal of Robotics Research, Vol.3, No.2, pp.60-72, 1984.

[11] Sano, A. and Furusho, J. , "Realization of Natural Dynamic Walking Using The Angular Momentum Information," Proc. of ICRA1990, Cincinnati, 3, pp.1476-1481, 1990.

[12] Nishiwaki, K., Nagasaka, K., Inaba, M. and Inoue, H., "Generation of reactive stepping motion for a humanoid by dynamically stable mixture of pre-designed motions," Proc. of 1999 Int. Conf. on Systems, Man, and Cybernetics, No. VI, pp.702-707, 1999.

[13] Pratt, J., Dilworth, P. and Pratt, G., "Virtual Model Control of a Bipedal Walking Robot," Proc. of the 1997 ICRA, pp.193-198, 1997.

[14] Raibert, M., *Legged Robots that Balance*, Cambridge, MA, MIT Press, 1986.

[15] Yamaguchi, J.,Soga,E., Inoue, S. and Takanishi, A., "Development of a Bipedal Humanoid Robot – Control Method of Whole Body Cooperative Dynamic Biped Walking –," Proc. of the 1999 ICRA, pp.368-374, 1999.

[16] Voyager Project Home Page, http://vraptor.jpl.nasa.gov/voyager/voyager.html

[17] Zheng, Y.F. and Shen, J., "Gait synthesis for the SD-2 biped robot to climb sloping surface," IEEE Trans. Robotics and Automation, vol.6, no.1, pp.86-96, 1990.